# Electrostatic effects on pressure drop in tube flows

**D. A. Nelson, M. M. Ohadi, S. Zia and R. L. Whipple**
Mechanical Engineering—Engineering Mechanics Department, Fluids Research Oriented Group, Michigan Technological University, Houghton, MI, USA

Electrohydrodynamic effects on forced convection in tubes may have significant implications for enhancement of heat exchanger performance in heat pumps and other devices. Of particular concern in such applications is the possibility of increased pressure drop associated with electrostatic discharge. Large frictional losses could substantially increase the required pumping power, offsetting performance gains associated with improved heat transfer rates.

This article describes a series of experiments designed to determine the effects of corona discharge on pressure fields for air flow in cylindrical tubes. Experiments were performed with a single concentric electrode in the tube and with two nonconcentric electrodes. Measurements were performed at potentials from the onset of measurable current to near the spark-over point and at Reynolds numbers from $10^3$ to $2 \times 10^4$. Friction factors were seen to increase as much as 250 percent over the values obtained in the absence of an applied electric field. Results suggest that the electrostatic effect on pressure drop is very sensitive to current density, Reynolds number, and electrode configuration.

**Keywords:** electrohydrodynamics; electrostatic pressure; Sentfleben effect

## Introduction

The "corona wind" that results from electrostatic discharge in a dielectric fluid can substantially alter pressure and flow characteristics under some conditions. Typically, the electric force on the fluid is relatively weak, to the extent that electrostatic pumping of a gas is a very inefficient process.[1]

Under certain conditions, it is possible to generate significant secondary motions in a flow by applying an electric field.[2,3] These secondary motions may substantially affect heat or mass transfer rates.[4–6]

The ability to materially increase convective heat transfer rates by means of electrostatic discharge may have practical applications for certain gas–gas or gas–liquid heat exchangers. This ability may be particularly true when compact size requirements result in an operating range characterized by modest Reynolds number values, making electrostatic enhancement viable. As with any enhancement technique, this one may carry a penalty in the form of increased pressure drop for the flow and a resulting increase in the pumping power requirement. The magnitude of the pressure drop associated with electrostatic discharge for a particular flow is sensitive to electrode geometry and polarity, current density, and flow conditions.

In this article we address the effects of electrostatic, or corona, discharge on the pressure drop for air flow in tubes. Attention is restricted to discharge from positively charged electrodes. Friction factors are obtained for both single- and dual-wire electrode configurations at Reynolds numbers ranging from $1 \times 10^3$ to $2 \times 10^4$ and at electrode potentials from the onset of corona discharge to near the spark-over voltage.

Address reprint requests to Professor Nelson at the Department of Mechanical Engineering, Michigan Technological University, Houghton, MI 49931, USA.

Received 24 March 1990; accepted 25 June 1990



## Methods

Measurements of pressure drop were performed for air flow using the induced-draft, flow-through system shown in Figure 1. The system consisted of a grounded aluminum tube with one or more stainless steel electrodes mounted longitudinally in the tube. Additional details of the system design are found in Reference 5.

### *Tube sections*

Room air was drawn through a 302-cm length of aluminum tube (3.2-cm i.d.). The tube was divided into three sections: a 159-cm entrance section, a 102-cm test section, and a 41-cm exit section. The entrance, test, and exit tube sections were electrically insulated from each other by plexiglass spacers of the same internal diameter as the tube. Mating surfaces were reamed and polished to eliminate any steps at the junctions. The interior tube surfaces were lapped to ensure smoothness.

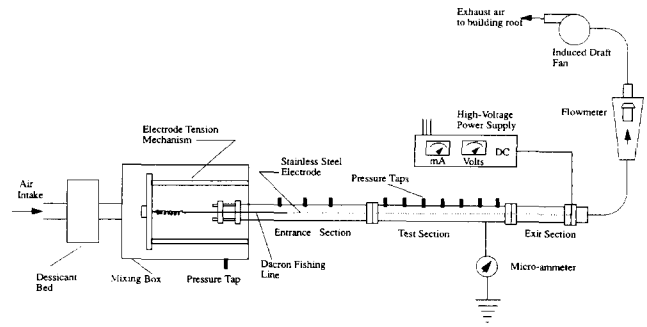


*Figure 1* System for measuring pressure drop for corona discharge in tube flows

The establishment of separate entrance, test, and exit sections was designed to minimize end effects on the electric field in the test section, producing a potential gradient that was almost uniformly radial within the test section. Electrical isolation of the respective sections allowed independent measurement of the current in each section. Further, the substantial entrance section length (equivalent to 50 tube diameters) allowed for flow development. Based on a hydrodynamic entry length $x_{fd}=0.05\mathrm{Re}_D D$,[7] the flow in the test section may be assumed to be fully developed for $\mathrm{Re}_D$'$1.4\times10^3$.

Pressure taps were drilled at 22-cm intervals in the entrance section, with the first tap 16 cm from the entrance section inlet. Taps were drilled at 3.2-cm intervals throughout the length of the test section, with the first tap position 9.5 cm from the upstream end of the test section. Each pressure tap was connected to a variable-capacitance, precision pressure transducer by a rotary switch specially designed and built for this application.

Inlet air was conditioned to 10–15 percent relative humidity by passing it through a desiccant bed ($CaSO_4$, 95%) upstream from the mixing box. Humidity was monitored with a dewpoint hygrometer.

### Wire electrodes

The wire electrodes consisted of 205-cm lengths of 0.25-mm diameter, 30 AWG stainless steel (AISI 304), running the length of the test section and extending 43 cm into both the entrance and exit sections. Each electrode was "aged" under tension for several hours prior to installation. This procedure eliminated residual kinks or bends in the wire.

At the upstream end, each electrode was joined to a length of braided dacron fishing line that connected to a spring-loaded electrode tensioning mechanism. The dacron fishing line served to suspend the electrode(s) in the tube while electrically isolating the electrode from the tensioning mechanism. A smooth glue joint connected the dacron to the electrode. The other end of the dacron line was attached to a support bracket.

The tensioning mechanism maintained a force of 11 N on the wire. This tension was sufficient to prevent measurable sagging of the electrode but was not large enough to stretch it significantly. The entire mechanism was housed in an insulated aluminum mixing box.

Corona discharge was obtained with a high-voltage, dc power supply connected to the wire electrodes. The power supply was capable of providing currents of up to 15 mA at 30 kV. The currents in the entrance, test, and exit sections were measured separately with a digital multimeter between the tube and earth ground.

Experiments were performed using both single-wire and two-wire electrode configurations. In the single-wire system, the wire electrode was concentric with the tube, which was grounded. Separate experiments were performed with the wire as the cathode and as the anode.

In the dual-wire configuration, the wires were positioned in the horizontal plane passing through the tube center axis, with each wire four millimeters from the center axis. Each wire was thus 12 mm from the tube wall. The wires were maintained at identical electrical potentials, and the tube wall was grounded.

### Results

For the single-electrode configuration, pressure data were obtained at three different electrode potentials—and ground—for each Reynolds number considered. The three potentials correspond to: (1) a potential slightly above the threshold voltage for the onset of corona; (2) a potential intermediate to the threshold and spark-over voltages; and (3) a potential slightly below the spark-over voltage. The voltages were preselected from the current–voltage data ($I$–$V$ curves) obtained under no-flow conditions.

For the dual-electrode configuration, data were obtained at four different electrode potentials—and ground. The potentials corresponded to voltages slightly above threshold and slightly below spark-over, as well as two intermediate potentials.

For both configurations, data were obtained at each of the preselected voltages at ten Reynolds numbers, ranging from $\mathrm{Re}_D=10^3$ to $2\times10^4$ (based on the inner diameter of the tube). For the conditions prevailing in these experiments, the Reynolds number range corresponded to volumetric flow rates of approximately $4\times10^{-4}$ m$^3$/s to $8\times10^{-3}$ m$^3$/s (0.8 ft$^3$/min to 16 ft$^3$/min).

### Current and voltage measurements

Preliminary current–voltage data were obtained under no-flow conditions and used to select electrode potentials for the experiments. For situations in which the convection contribution to total current is small, the current density should be independent of fluid velocity. Formally, this condition requires $U/(\beta E)\ll1$,[8] where $U$ and $E$ are the nominal fluid velocity and electric field magnitudes and $\beta$ is the ion mobility.

For discharge from a single electrode at a potential of 7.0 kV, concentric to a 3.2-cm diameter tube, the requirement $U/(\beta E)\ll1$ limits the nominal fluid velocity to $U<7.9\,\mathrm{m\cdot s^{-1}}$, or $\mathrm{Re}_D<1.6\times10^4$. Thus to leading order, the voltage–current relationship should be independent of the flowrate at all but the largest Reynolds numbers examined. Although there were some observed variations in the average current obtained at a given voltage, no clear dependence on Reynolds number was discerned.

### Pressure data

Pressure was measured at each tap with respect to the static pressure in the mixing box. Pressure data are reported in the

## Notation

| | |
|---|---|
| $D$ | Tube inner diameter |
| $E$ | Electric field magnitude |
| $f$ | Friction factor |
| $f_{E\neq0}$ | Friction factor obtained with applied electric field |
| $f_{E=0}$ | Friction factor obtained with zero applied electric field |
| $F_{e_i}$ | Electric body force vector |
| $J_i$ | Current density vector |
| $K_p(x)$ | Pressure coefficient at axial location $x$ |
| $P_0$ | Pressure in mixing box at tube inlet |
| $P(x)$ | Pressure |
| $\mathrm{Re}_D$ | Reynolds number based on tube inside diameter |
| $U$ | Nominal fluid velocity |
| $u_m$ | Mean air velocity in the tube |
| $x_{fd}$ | Hydrodynamic entry length |

*Greek symbols*

| | |
|---|---|
| $\beta$ | Ion mobility |
| $\phi$ | Electrode potential |
| $\rho$ | Mass density of air |

form of a dimensionless pressure coefficient $K_p(x)$, defined by

$$K_p(x)=\frac{P_0-P(x)}{\frac{1}{2}\rho u_m^2}$$

where

$P_0$ = pressure in mixing box at tube inlet;
$P(x)$ = pressure at tap at axial location $x$;
$\rho$ = mass density of air; and
$u_m$ = mean air velocity in the tube.

Figures 2 and 3 present pressure coefficients for $Re_D$ = 2,000 for the single-electrode and dual-electrode configurations, respectively. Pressure coefficients obtained at $Re_D$ = 5,000 for the two configurations are presented in Figures 4 and 5. In each case, the pressure coefficients are plotted as a function of dimensionless distance from the system inlet ($x/D$). Corresponding data were obtained at each of the other eight Reynolds numbers investigated.

For purposes of data presentation, the tube length was divided into entrance (I) and test (II) regions. The entrance region was subdivided into the section containing the dacron line (IA) and the section containing a portion of the electrode (IB).

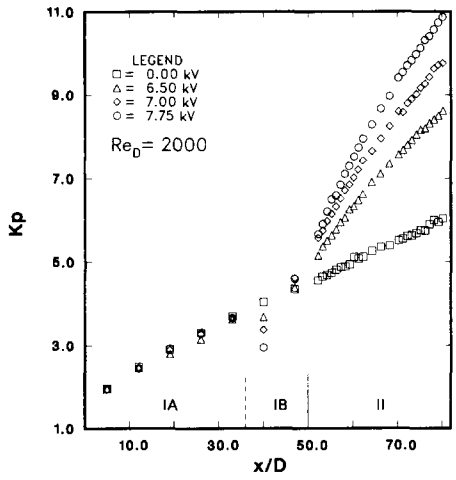


*Figure 2* Pressure coefficient as a function of tap location at $Re_D$ = 2,000 for discharge from a single electrode, concentric with the tube

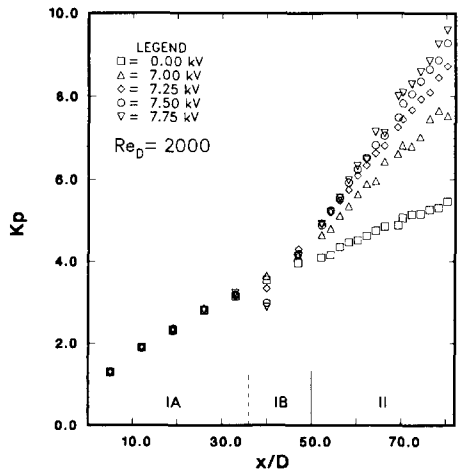


*Figure 3* Pressure coefficient as a function of tap location at $Re_D$ = 2,000 for discharge from two nonconcentric electrodes

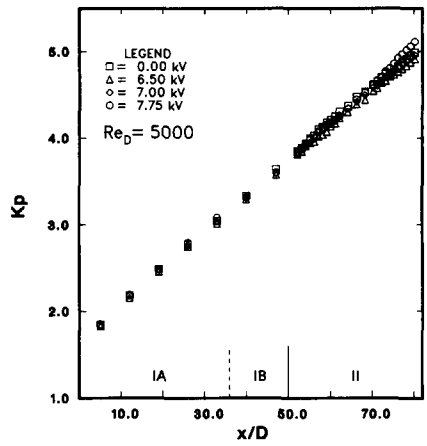


*Figure 4* Pressure coefficient as a function of tap location at $Re_D$ = 5,000 for discharge from a single electrode, concentric with the tube

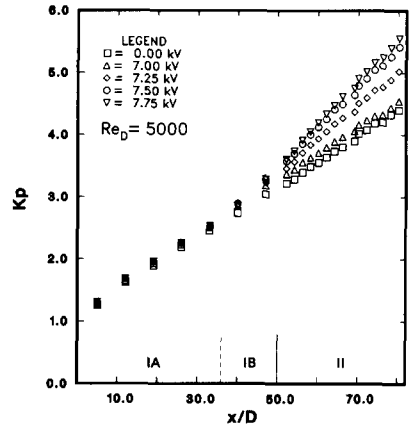


*Figure 5* Pressure coefficient as a function of tap location at $Re_D$ = 5,000 for discharge from two nonconcentric electrodes

At $Re_D$ = 2,000, Figures 2 and 3 indicate a discontinuity in the pressure gradient at a location coincident with the dacron–electrode junction. This discontinuity may be attributed to the electric body force, which would tend to increase the pressure throughout the energized region. This effect was seen at Reynolds numbers up to $Re_D$ = 4,000, although the jump magnitude diminished at the higher Reynolds numbers.

## *Friction coefficients*

Pressure gradients are reported in the form of a dimensionless friction factor, $f$, defined as:

$$f=-\left(\frac{2D}{\rho u_m^2}\right)\frac{dP}{dx}$$

where $dP/dx$ was obtained from a least-squares linear fit to the pressure data obtained in the test section (section II in Figures 2–5).

Uncertainty in friction factor results is caused by a combination of measurement error and error introduced by the least-squares fit to the pressure data. The uncertainty associated with each of these contributions is a function of Reynolds number. At low $Re_D$ values, pressure variations in the test section were very sensitive to laboratory conditions and required a long equilibration time for the system.

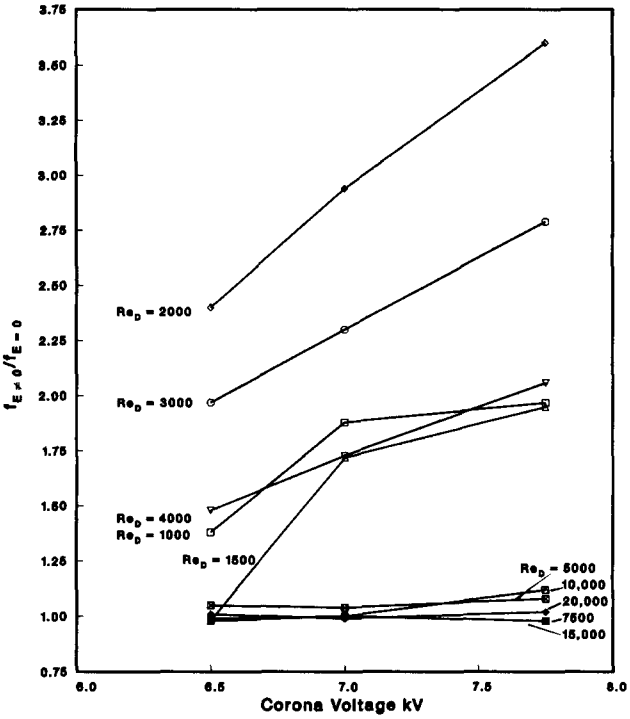


*Figure 6* Relative friction factor as a function of electrode potential for discharge from a single electrode, concentric with the tube

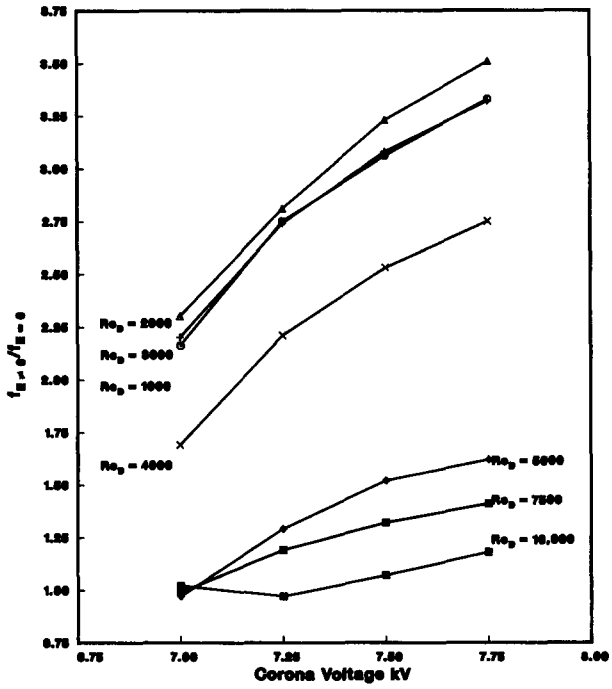


*Figure 7* Relative friction factor as a function of electrode potential for discharge from two nonconcentric electrodes

The average compounded uncertainty for the friction factor ranged from 4.1 percent at $Re_D = 1{,}000$ to 13.8 percent for $Re_D$(10,000. Details of the uncertainty analysis may be obtained from Professor Nelson.

Figure 6 displays the ratio of the friction factor obtained during corona discharge to that obtained with no applied field for the single-electrode configuration. The ratio is plotted against the voltage maintained between the wire electrode and the grounded tube wall. Figure 7 shows the corresponding results for the dual-electrode configuration, in which both wires are maintained at the same positive potential with respect to the tube wall.

## Discussion

At $Re_D = 2{,}000$, both the single- and dual-electrode configurations show elevated pressure coefficients with higher electrode potentials. This result implies an increasing rate of pressure drop with increasing electric body force. At $Re_D = 5{,}000$, discharge from a single electrode (Figure 4) has little effect on the rate of pressure drop. However, simultaneous discharge from two electrodes (Figure 5) produces a substantial effect on the rate of pressure drop in the tube. This increased effect with the dual-electrode configuration may be attributable to geometric effects or to the higher currents obtained with discharge from two electrodes.

The electric force responsible for the observed pressure effects is the result of the Coulomb force acting on the positive ions, which are produced in the corona discharge zone in the immediate vicinity of the wire(s). The electric force is imparted to the neutral gas molecules through collisions between ions and neutral molecules.[9] Assuming negligible charge carrier convection, we can write the electric body force $F_{e_i}$ here as

$$F_{e_i} = \frac{J_i}{\beta}$$

where $\beta$ is the ion mobility in the fluid.

A comparison of the relative increases in the friction factor for the single- and dual-electrode configurations is shown in Figure 8. The friction factor is plotted against the measured test section current for selected Reynolds number values. These

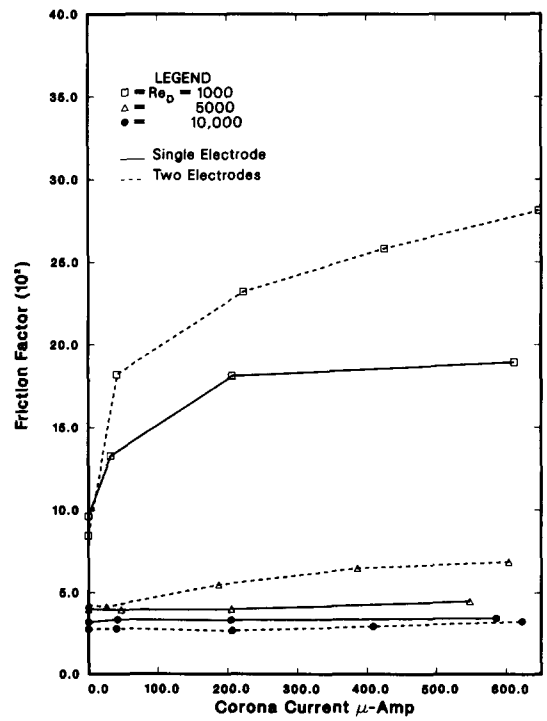


*Figure 8* Comparison of friction factors for single- and dual-electrode configurations at selected Reynolds numbers

representative results illustrate that the dual-electrode configuration generally has a greater effect on the pressure drop for a given current density. At $Re_D = 5{,}000$, the dual-electrode system produces a marked increase in the friction factor, whereas no significant electric effect is associated with discharge from a single electrode at $Re_D = 5{,}000$. At high Reynolds numbers ($Re_D = 10{,}000$, Figure 8), neither configuration significantly affects friction factors electrically.

This geometric effect can be attributed to the nonconservative current density field produced by the dual-electrode configuration. If we assume that discharge is spatially uniform from a single, coaxial electrode, the resulting current distribution produces a force field that is wholly irrotational. Although this force field would effect a radial pressure gradient in the tube, it would not affect the flow pattern.[8] The significant increase in the longitudinal pressure gradient observed with a discharge from a single coaxial electrode (compared to the pressure drop in the absence of any discharge) is due to the fact that the discharge is not spatially uniform; it occurs at discrete locations along the electrode.

The increased effect associated with discharge from two electrodes is caused in part by the greater degree of irrotationality of the electric body force when compared with the force field resulting from single-electrode discharge.

The electrostatic effect on pressure drop is highly sensitive to Reynolds number, as suggested by Figures 6 and 7. The relative increase in the friction factor is generally greatest for flows in the laminar and transition regimes. For both electrode configurations, the greatest relative increase in the friction factor was observed at $Re_D = 2{,}000$. One interpretation of this result is that the electrostatic discharge promotes transition from laminar to turbulent flow, thereby increasing the pressure drop most dramatically at Reynolds numbers near the critical value.

For both configurations examined, the effect is greatly diminished in the case of fully turbulent flow. This result is consistent with previously observed electrostatic effects on transport rates, which show that such effects are generally slight at $Re_D > 5{,}000$.[4] The diminution of electrostatic effects in fully turbulent flows is not surprising, as the effect is associated with an electrical contribution to secondary flows. At higher Reynolds numbers, inertial forces are large compared to the electric force. Thus the relative contribution of electric forces is reduced at large $Re_D$.[10]

## Conclusions

Clearly, corona discharge may produce large increases in frictional losses (thus increasing required pumping power). This result is particularly significant at Reynolds numbers in the laminar and transition regimes. However, the role of electrode geometry should not be overlooked when considering the electrostatic effects on pressure drop. A geometry that produces a strongly rotational current density field may yield effects that are greater in magnitude—and extend to higher Reynolds numbers—than would be obtained with a largely irrotational current distribution. Whether other transport rate effects (i.e., heat transfer and mass transfer enhancement) are similarly sensitive to electrode geometry is currently being investigated.

## Acknowledgments

This work was supported by the Gas Research Institute under Contract No. 5087-260-1528.

## References

1 Robinson, M. Movement of air in the electric wind of the corona discharge. *Trans. AIEE*, 1961, **80**, 143–150

2 Fernandez, J. L. Electrohydrodynamic enhancement of forced convection heat transfer in tubes. Ph.D. dissertation, University of Bristol, UK, 1975

3 Franke, M. E. Effect of vortices induced by corona discharge on free-convection heat transfer from a vertical plate. *J. Heat Transfer*, 1969, **91**, 427–433

4 Kulacki, F. A. Electrohydrodynamic enhancement of convective heat and mass transfer. In *Advances in Transport Processes*, vol. II, A. S. Mujumdar and R. A. Mashelkar, eds. John Wiley & Sons, New York, 1982

5 Nelson, D. A. and Ohadi, M. M. EHD enhancement of heat transfer in heat exchangers. Report GRI-88/0194, Gas Research Institute, Chicago, IL, 1988

6 Franke, M. E. and Hutson, K. E. Effects of corona discharge on the free-convection heat transfer inside a vertical hollow cylinder. *J. Heat Transfer*, 1984, **106**, 346–351

7 Incropera, F. P. and DeWitt, D. P. *Fundamentals of Heat and Mass Transfer*, 2nd ed. John Wiley & Sons, New York, 1985, 369

8 Nelson, D. A. and Shaughnessy, E. J. Electric field effects on natural convection in enclosures. *J. Heat Transfer*, 1986, **108**, 749–754

9 Yabe, A., Mor, Y., and Hijikata, K. EHD study of the corona wind between wire and plate electrodes. *AIAA J.*, 1978, **16**, 340–345

10 Davidson, J. H., Kulacki, F. A., and Dunn, P. F. Convective heat transfer with electric and magnetic fields. In *Handbook of Single-Phase Convective Heat Transfer*, S. Kakaç, R. K. Shah, and W. Aung, eds. John Wiley & Sons, New York, 1987